Structural behavior of concrete-filled steel tubular (CFST) with spherical cap gap subjected to corrosion and long-term tensile loading

Simin Tang, Yuxing Yang, and Feiyu Liao*

College of Transportation and Civil Engineering, Fujian Agriculture and Forestry University, Fujian 350108, China

Abstract. Concrete-filled steel tubes (CFSTs) are commonly used as structural specimens in construction. Gaps between the steel tube and enclosed concrete core can form during manufacture or repair procedures. This study developed a computational model to investigate the structural implications of spherical cap gaps in CFSTs subjected to sustained axial tension and chloride-induced corrosion. Finite element analysis (FEA) incorporated appropriate material constitutive laws and elements. Model predictions closely matched experiments for load-displacement response and ultimate capacity. Parametric comparisons between gap and no-gap geometries quantified performance impacts, including reduced stiffness, deteriorated load transfer, internal force redistribution, and diminished flexibility stemming from localized steel tube buckling adjacent to the unrestrained gap. Outcomes highlight the importance of quality control during CFST production and repair to minimize defects like uncoupled zones between the concrete infill and hollow tube. The validated simulation approach provides an efficient tool for exploring gap influences and informing structural design provisions.

1 Introduction

China is rapidly developing into a maritime power, necessitating major sea-related infrastructure to support the burgeoning coastal economic centers. Steel-tube concrete composite structures are frequently utilized as the primary load-bearing structures in such projects, owing to their exceptional mechanical properties, convenience of construction, and economic advantages [1]. However, the typical casting method for CFSTs in arch bridges and trusses can create structural issues. The concrete is gradually poured from the bottom up, often resulting in air voids or bleed water near the top. Differential settlement and shrinkage also introduce gaps at the interface, known as "spherical cap gaps" [2]. These flaws undermine the composite action between the steel tube and concrete, posing safety hazards. Furthermore, the humid marine environments and sustained heavy loading can accelerate the corrosion of the steel tubes throughout the structure's service life.

Previous studies have examined the mechanical deficiencies introduced by spherical cap gaps and corrosion in concrete-filled steel tubes (CFST). Liao [3] performed axial tension tests on CFSTs with gaps, finding reduced composite action and load capacity compared to fully bonded specimens. Complementary analysis by Lin [4] further described the theoretical effects of gaps under long-term loading. Additionally, the concrete core's time-dependent response influences behavior, with shrinkage and creep affected by concrete mix, size, loading duration, etc. [5,6]. Han [7] studied coupling effects between sustained tension loads and chloride corrosion using accelerated tests and finite element analysis. Despite corrosion damage, the steel and concrete maintained composite interaction, demonstrating the structure's redundancy. However, gaps and corrosion both undermine critical CFST performance, necessitating durability improvements. In summary, prior works have quantified individual and combined impacts but further study of interacting parameters and effects on safety factors is merited. Enhanced quality control during casting along with corrosion-resistant coatings could mitigate primary deficiencies observed thus far.

In summary, CFST members with gap defects in the marine environment are subjected to the combination of chloride corrosion and long-term loading from the start of their service life. This results in a significant change in stress levels and mechanical properties of the CFST, which exhibit a non-linear characteristic with the increase of corrosion thickness. These changes have an impact on member stresses that require further investigation. It is of immense theoretical significance and practical engineering value to carry out a study of the mechanical properties of CFST axial tension specimens with spherical cap gaps under the combination of ion corrosion and long-term exposure. This paper conducts a complete force analysis of the specimens, summarizes the redistribution laws of internal force, and compares the destruction morphology of different specimens under different working conditions to clarify the force mechanism.

* Corresponding author: feiyu.liao@fafu.edu.cn

2 FEA modelling.

2.1. Material constitutive model

The constitutive model of the steel material uses a five-stage quadratic plastic flow model by Han et al [7], which satisfies both the *von Mises* yield criterion and the isotropic hardening criterion. In the FEA model, the elastic modulus E_s of the steel material is 206000 MPa, and the Poisson's ratio is 0.3.

The CFST relies on composite interaction between steel tube and concrete. Han [7] proposed using a plastic damage model to characterize the confined concrete core. This employs the uniaxial stress-strain relationship in compression to account for restraint from the steel tube. For tension, a fracture energy crack model describes the post-peak softening response. The cracking stress (σ_{t0}) calculation originates from Han's [7] formula for concrete tensile capacity. In summary, the model captures key composite behaviors including triaxial compression enhancement and tension stiffening. Validating the simulations with additional physical tests across a range of parameters would further improve confidence. Quantifying the interface bond strength and its degradation over time may better represent the aforementioned gaps observed in practice.

2.2 Description of the FEA modelling.

To simulate the thickness variation of the outer steel tube for corrosion modelling, we used an 8-node 3D solid element with reduced integration (C3D8R) for the unit types of the steel tube, the core concrete, and the end plate. To simulate the loss of thickness of the outer steel tube, a technique called '*Model change, remove*' was employed for the corrosion of the outer tube. The steel tube was divided into two layers of solid units along the thickness direction. The outer layer of solid units represented the actual thickness of the corroded section, and the inner layer of units corresponds to the remaining thickness of the steel tube after corrosion. The two-layer solid element was constrained using "Coupling" to guarantee that the elements of both layers work in unison. The outer solid element of the steel tube was "deactivated" during the corrosion process, so that the stiffness of the outer element was gradually reduced to zero, simulating the loss of thickness on the outer wall of the steel tube. The grid density is determined by the grid experiment.

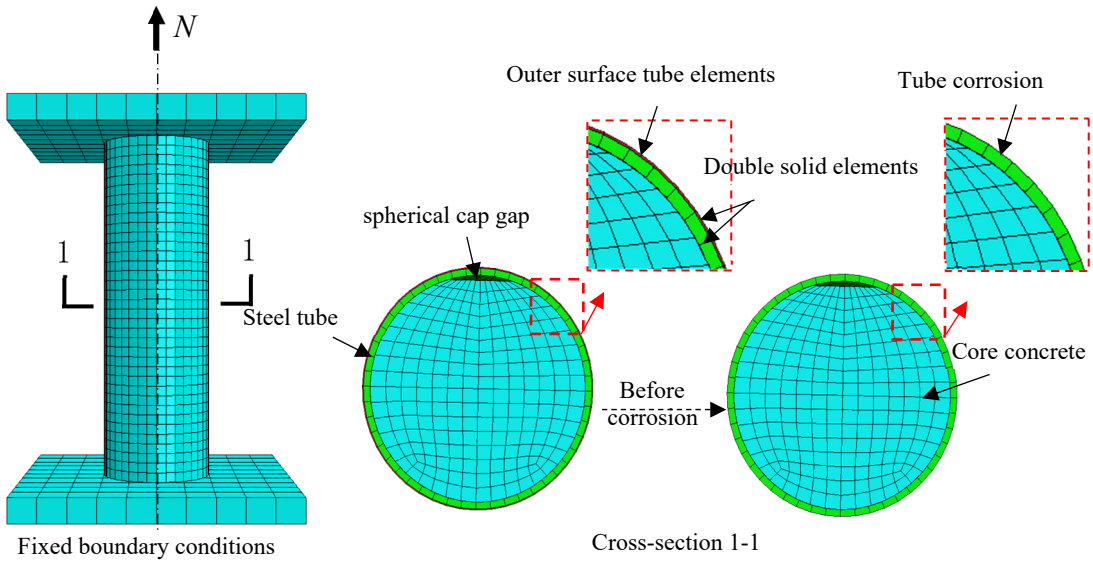

Fig.1 Schematic diagram of FEA model of CFST axial tension specimen

The interface behavior between the steel tube and core concrete was modeled using a coulomb friction contact in the tangential direction (friction coefficient = 0.6) [7] and a hard normal contact allowing detachment but prohibiting embedment [7]. Separation was not considered since the steel's higher Poisson's ratio constrains the concrete in tension. While important for ultimate limit states, the bond strength effect was excluded from the post-corrosion analysis focused on damage progression. Justification should be provided if debonding initiation/propagation is neglected, as gaps compromise composite action. Quantifying slip and separation in the model could better represent observed deficiencies while still excluding shear transfer mechanisms. Additionally, calibrating the friction coefficient against physical push-through tests can improve accuracy during cyclic and reversed loading. In future works, explicitly modeling the interface as a zero-thickness cohesive element may enable capturing progressive bond degradation induced by durability factors and loads.

For the boundary conditions, reference points were set at the two end plate surfaces to couple with the end plate surfaces, and end plate constraints were applied at one end to constrain the displacements and rotations in all directions. At the other end, all displacements and rotations were constrained except for the axial concentrated load applied.

2.3 Finite Element Analysis (FEA) models

Figure 1 shows a schematic of the FEA model of the CFST axial tension specimen. The diagram illustrates the

analysis that incorporated long-term loading and corrosion effects using a two-model approach. Model I applied the sustained axial load (N_l) first via static analysis. Next, concrete shrinkage and creep were introduced using a 3D viscoelastic model with the standard linear solid theory [9]. The peak strain was amplified by a factor of 1.9 to account for creep per Han [10]. After 100 days, creep stabilizes [8], so this was the step length.

Model II initialized from Model I's state. First, the steel tube thickness was reduced to simulate chloride corrosion damage based on time-dependent penetration relationships. Then, displacement-controlled tension was applied until failure. Stress redistribution and deterioration of composite action due to the degraded interface were thus captured.

While using two sequential models improves computational efficiency, results may be mesh-dependent. Adaptive re-meshing techniques could enable modeling the full duration within one model. Explicitly defining the corrosion-induced interface gaps and bond strength degradation could better match observations. Quantifying the impacts on ductility and residual capacity will inform structural integrity assessments and maintenance plans for aging CFST infrastructure in marine environments.

2.4 Validation of the FEA model

Before the FEA analysis was carried out, experimental research was carried out on CFST elements with a spherical cap gap. The specimens were subjected to accelerated corrosion by electrical means in a chloride ion solution and were subjected to a constant axial tensile load for 120 days. After completion of the long-term loading and corrosion stages, the specimen from the long-term loading device. The steel tubes were stripped of the water tank and strain gauges were attached to the surface of the steel tubes. The samples were relocated to a 200-ton hydraulic servo universal testing machine and tested for failure.

To confirm the model's applicability, numerical simulations were performed on the experiments using the aforementioned model. The compressive strength of concrete cubes (f_{cu}) measured 53.19 MPa, and the yield strength of steel material (f_y) was 473.7 MPa. The sectional of the member is $D\times t$=121×4 mm, where the outer section diameter of the CFST member is D and the wall thickness of the steel tube is t. The length of the specimens is 360 mm. Figure 2 illustrates the load-displacement (N_t-Δ) curves of typical CFST specimens obtained from the experiments and calculations. In the diagram, Δt is the corrosion depth of the external steel tube and n is the long-term load ratio ($n=N_l/N_u$, where N_l represents the long-term loading and N_u denotes the calculated load carrying capacity of the specimen), χ is the spherical cap gap ratio ($\chi=d_s/D$, where d_s is the value of the spherical cap gap). Upon comparing the analysis results, a high correlation is found between the calculated results and the experimental results.

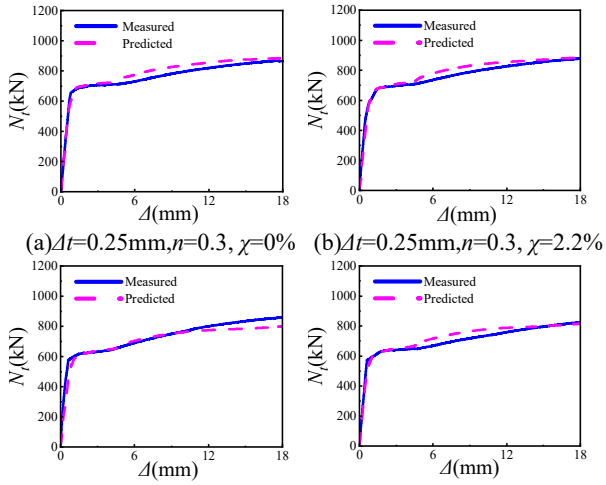

(a)Δt=0.25mm,n=0.3, χ=0% (b)Δt=0.25mm,n=0.3, χ=2.2%

(c)Δt=0.62mm,n=0.3,χ=2.2% (d)Δt=0.56mm,n=0.6,χ=2.2%

Fig.2 N_t versus Δ relations of CFST tensile specimens under corrosion and long-term loading

3 Analysis of the working mechanism

3.1 Analytical Behavior

Using the FEA model above, this section analyses the effect of a spherical cap gap on the working mechanism of CFST specimens under long-term axial tensile loading and corrosion. It analyses the destruction morphology of the specimens, the load-displacement curve, the internal forces between the steel pipe and concrete redistributed., and the interactions between the two cross-sections. Typical parameters for calculation are as follows: $D\times L\times t$=400×1200×9.3mm, the long-term load ratio of 0.5, the corrosion thickness is 2.79 mm, and the spherical cap gap of 4.4%, f_{cu} measured 60 MPa and f_y was 345 MPa.

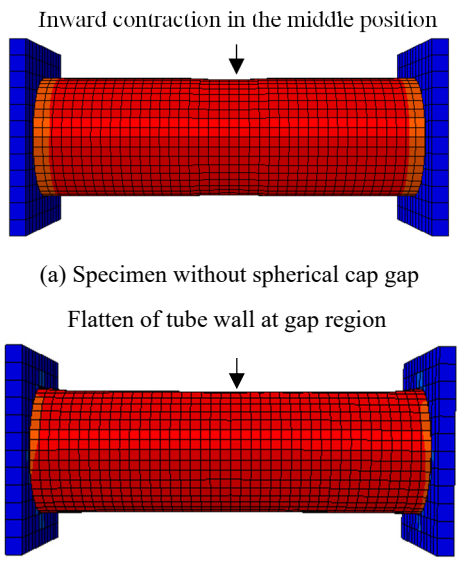

(a) Specimen without spherical cap gap

(b) Specimen with spherical cap gap (χ=4.4%)

Fig.3 Comparison of typical failure modes

Figure 3 compares the failure modes between the specimen without gaps and the one with a spherical cap gap under coupled corrosion and loading. For the fully composite member, the core concrete supports the steel tube internally, restricting deformation. However, on the

gap side, the missing concrete allows premature localized buckling and severe flattening of the steel tube. The opposite side resembles the no-gap specimen since composite interaction remains intact.

This highlights the significant impact of even partial interface deficiencies on ductility and failure progression. The exposed steel on the gap side undergoes stress concentrations and increased proportional loading. Capturing this localized damage and material deterioration in the model could better match the asymmetrical failure observed. Explicitly defining the void thickness and area may improve accuracy compared to simply removing elements. Overall, maintaining complete contact and bonding between steel and concrete during casting and service is critical to ensure composite benefits in these structures.

3.2 Load-Displacement Relations

To facilitate the analysis of the role of concrete in CFST with a gap under the combined influence of corrosion and loading, the following four calculations were selected for comparison, as shown in Figure 4: A: short-term loaded CFST specimens; B: short-term loaded CFST specimens with spherical cap gap; C: CFST specimens under combined corrosion and loading; D: CFST specimens with spherical cap gap under combined corrosion and long-term loading. For structures with no considerable long-term corrosion, the stiffness during the service phase corresponds to a cut-line stiffness of 0.6 N_t, whereas the initial loading stiffness is defined as the cut-line stiffness corresponding to 0.3 N_t. For specimens under long-term corrosion conditions, the service phase stiffness is the cutline stiffness corresponding to the state after the long-term load-holding phase and before the onset of destructive loading [9].

The calculations demonstrate that the specimen's initial loading stiffness and service phase stiffness decreased by 13.7% and 5.3%, respectively, after accounting for the influence of the spherical cap gap. The carrying capacity has decreased by 3.9%. , which is deemed insignificant. The effect of the spherical cap gap created during construction on stiffness is obvious; however, it gradually diminishes under increased load, and the effect on load-carrying capacity is negligible. Together with the effect of corrosion and loading, the initial load stiffness and service stiffness of the member decreased by 17.5% and 34.4% respectively, with a significant decrease in stiffness attributed to the fact that the steel tubes in the axial tension members essentially took all the axial tension loads. At the same time, the combined process of corrosion and loading significantly reduces the load-carrying capacity of the specimens, and compared with the short-term loading of CFST specimens, it decreases by 31.5% for the non-gap specimens and 33.6% for the spherical cap gap specimens, and the decrease in load carrying capacity of the non-gap specimens is lower than that of the spherical cap gap specimens. The reduction in thickness of the steel tube highlights the enhanced role of the concrete part. Additionally, the presence of the spherical cap gap further diminishes the role played by the concrete.

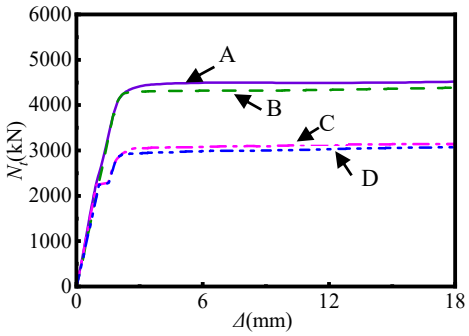

Fig. 4 Comparison of results of typical arithmetic specimens

3.3 Load Transfer Mechanism

Finite element analysis (FEA) was conducted to determine the distribution of axial tensile forces on the outer steel tube and inner concrete core of concrete-filled steel tube (CFST) sections, with and without spherical cap gaps, under combined corrosion and loading effects. The axial tensile bearing capacity N_t of the specimens was defined, following other researchers' criteria, as the load value corresponding to an axial tensile strain (ε) in the steel tube equal to 5000 με. Since the axial tensile strain is uniform along the length, ε can be approximated as Δ/L, where Δ is the elongation, and L is the specimen length.

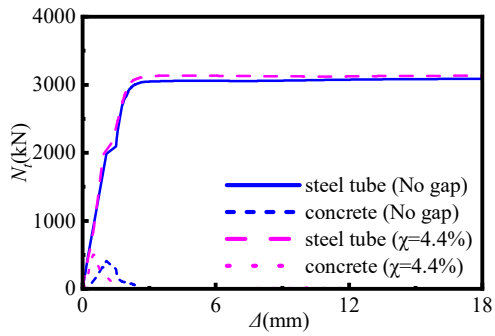

Fig. 5 Distribution of internal forces in CFST

As Figure 5 shows, the axial tensile force transferred to the concrete core is already decreasing during the initial loading phase for non-gapped specimens. In this early stage, longitudinal elongation of the outer steel tube causes relative displacement with the inner concrete. Resulting interfacial friction stresses transfer axial forces from the steel to the concrete, achieving load sharing between the two materials. In contrast, for specimens with gaps, the reduced steel-concrete contact area delays this load transfer due to the interface gap.

Figure 6 illustrates the force distribution for gapped specimens - initially, the outer steel tube carried 81.7% of the total axial tensile force, while the remaining 18.3% was borne by the concrete core. In the subsequent long-term load-holding phase, the model incorporated constitutive relations governing concrete behavior under sustained compression, including effects of shrinkage and creep. Results indicate internal force distribution and axial deformations remained largely constant during this period.

However, during the steel tube corrosion stage, thinning of the outer wall increased stress levels and

deformation. This led to a reduction in the tensile force carried by the concrete to 12.7%, while the steel tube bore 87.2%. In the final loading stage, upon reaching the concrete cracking stress, the core can no longer sustain tensile forces. At this point, load transfer across the steel-concrete interface shifts the entire tensile load to the steel tube.

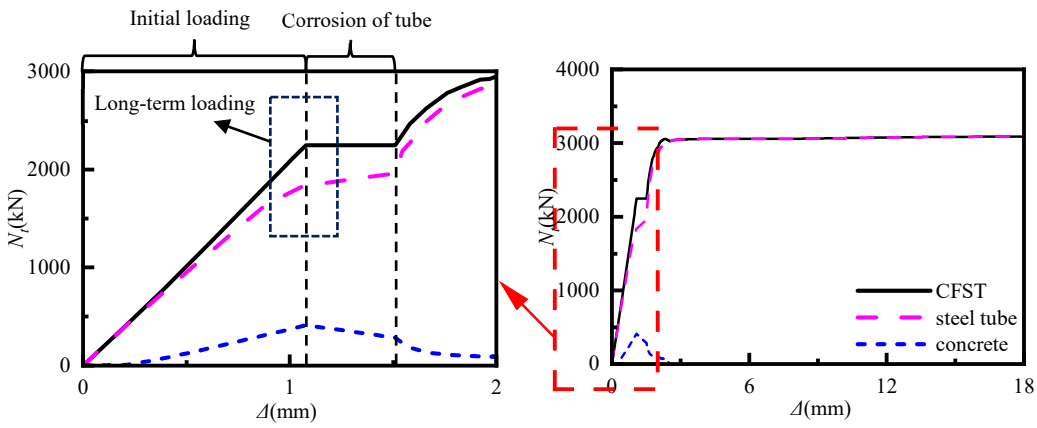

Fig. 6 Distribution of internal forces throughout the external steel tube and core concrete

3.4 Analysis of Contact Stress

FEA analysis was used to obtain the contact stresses σ - longitudinal strain ε curves at the characteristic points of the member spanning the mid-section. The locations of the characteristic points are shown in Figure 7. The analysis aimed to investigate the influence of corrosion and long-term axial tensile load on the interaction between the steel tube and core concrete.

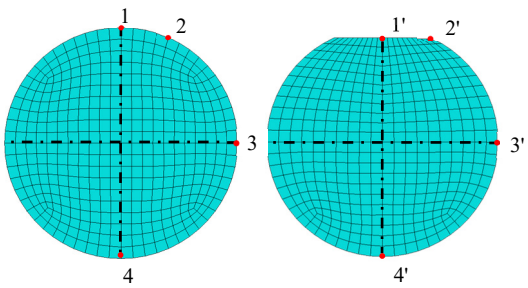

Fig. 7 Location of measurement points for contact stress

Figure 8 shows consistent behavior across four key characteristics for CFST axial tension specimens without gaps. Under loading, the steel tube and concrete achieve immediate contact. Stress builds rapidly, and upon reaching the concrete cracking threshold, cracks form as the stress drops to zero. With continued stretching of the CFST, the tube undergoes necking before re-contacting the concrete.

Figure 8(a) illustrates substantial differences between specimen's sunder long-term post-corrosion loading versus short-term loading. During the long-term phase, the deformation of the specimens increases significantly, creating noticeable hysteresis in the contact stress response and its subsequent development. At the end of corrosion, the contact stress decreasing phase is more prolonged, with a markedly reduced slope for the rising segment. The 5000 με limit state falls at the trough of this decreasing phase, 65.7% below the value for the non-corroded condition.

In the spherical cap gap member, at feature point 1', the contact stress was consistently zero, indicating that the internal steel tube and core concrete were not in contact throughout. This suggests that the concrete was not restrained by the steel tube in this region. The concrete cross-section undergoes an abrupt change in shape due to the presence of a spherical cap gap. , resulting in a significant stress concentration at characteristic point 2' in Figure 8 (b). Specimens with gaps experience much higher maximum contact stresses than those without. the contact stresses at measurement points 3' and 4' are significantly delayed compared to the non-gap specimens in Figs. 8 (c) and (d). The descending section is smoother, and the slope of the ascending section is significantly lower. The presence of the spherical cap gap blocks the path of load propagation from the steel tube to the core concrete, resulting in a delay in specimen contact and the mechanism of axial force transmission. The contact stresses at all locations, except the gap boundary, are generally lower than those of the corresponding non-gap specimens. In Fig. 8 (c), the values of contact stresses in the limit state of the short-term loaded specimens are weakened by an average of 54.2% compared to those of the non-gap specimens. The contact stress value of the long-term corroded member with a gap (point 3') is 1.49 MPa, while that of the non-gap (point 3) is 1.67 MPa, the restraining effect of the steel tube on the concrete in this region is reduced by the presence of the spherical cap gap. Figure 8(d) shows that the contact stress values in the limit state of short-term loaded specimens are weakened by an average of 43.3% compared to specimens without gap area. It is shown that the spherical cap gap also affects the confinement effect in the region away from the gap side, but less than in the intermediate region.

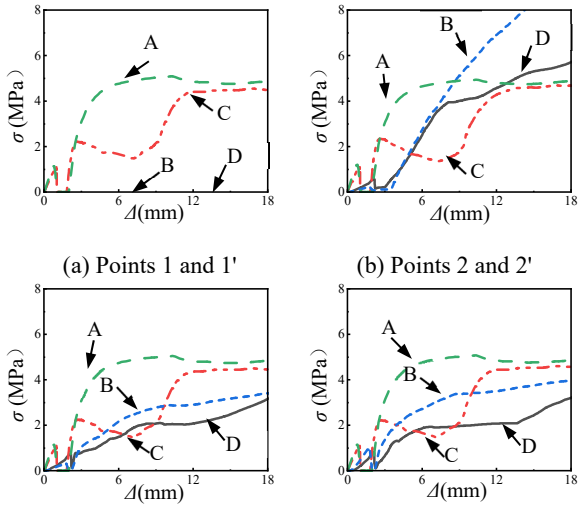

(a) Points 1 and 1' (b) Points 2 and 2'

(c) Points 3 and 3' (d) Points 4 and 4'

Fig. 8 Comparison of contact stress

4 Conclusions

This study presents a finite element model of CFST axial tension specimens with spherical cap gaps under combined long-term load and chloride ion corrosion. Validation against test data verifies the model's reasonableness. Comparative analyses and examination of the full-force response lead to the following key conclusions:

1. Gap-induced ovalization of the steel tube weakens concrete core support, reducing member capacity.
2. Once cracked, the concrete no longer directly bears axial tension forces. Gaps decrease the steel-concrete interface, delaying load transfer and strain development.
3. Gaps and corrosion reduce member stiffness and ultimate strength. Under equal conditions, non-gapped specimens exhibit smaller capacity losses, confirming the concrete's reduced role.

These results can guide performance evaluations and the design of CFST for marine environments.

References

1. Han, L. H., Mu, T. M., Wang, F. C., et al. (2020) Design theory of CFST(concrete-filled steel tubular)mixed structures and its applications in bridge engineering[J]. China Civil Engineering Journal,53(5): 1-24. DOI:10.15951/j.tmgcxb.20200413.001
2. Liao, F. Y., Han, L. H., He, S. H., (2011) Behavior of CFST short column and beam with initial concrete imperfection: Experiments[J]. Journal of Constructional Steel Research, 67(12): 1922-1935. https://doi.org/10.1016/j.jcsr.2011.06.009
3. Liao, F. Y., Li, Y. F., Rao, G. H., et al. (2021) Mechanical behavior and design approach of concrete filled steel tubes with circular − segment gap under combined actions of tension and bending[J]. Journal of Building Structures, 42(5), 165-176. DOI:10.14006/j.jzjgxb.2018.0676
4. Lin, T. W., (2018) Study on the Effect of Gap on the Static Behavior of Circular Concrete-Filled Steel Tubular (CFST)Members Under Long-term Loading[J]. Progress in Steel Building Structures, 20(2):74-78. DOI:10.13969/j.cnki.cn31-1893.2018.02.010
5. Naguib, W., Mirmiran, A., (2003). Creep modeling for concrete-filled steel tubes[J]. Journal of Constructional Steel Research, 59(11), 1327–1344. DOI:10.1016/S0143-974X(03)00085-3.
6. Kwon, S. H., Kim, T. H., Kim, Y. Y., et al. (2007) Long-term behaviour of square concrete-filled steel tubular columns under axial service loads[J]. Magazine of Concrete Research, 59(1), 53–68. https://doi.org/10.1680/macr.2007.59.1.53
7. Han, L. H., Hua, Y. X., Hou, C., et al. (2017) Circular Concrete-Filled Steel Tubes Subjected to Coupled Tension and Chloride Corrosion[J]. Journal of Structural Engineering, 143(10). https://doi.org/10.1061/(ASCE)ST.1943-541X.0001874
8. Han, L. H., He, S. H., Liao, F.Y., (2011) Performance and calculations of concrete filled steel tubes (CFST) under axial tension[J]. Journal of Constructional Steel Research, 67(11), 1699–1709. DOI:10.1016/j.jcsr.2011.04.005
9. Han, L. H., Li. Y., Liao, F. Y., (2011) Concrete-filled double skin steel tubular (CFDST) columns subjected to long-term sustained loading[J]. Thin-Walled Structures, 49(12): 1534-1543. DOI:10.1016/j.tws.2011.08.001
10. Han, L. H., Tao, Z., Liu, W., (2004) Effects of Sustained Load on Concrete-Filled Hollow Structural Steel Columns[J]. Journal of Structural Engineering, 130(9): 1392-1404. DOI:10.1061/(ASCE)0733-9445(2004)130:9(1392)